

JamMa: Ultra-lightweight Local Feature Matching with Joint Mamba

Xiaoyong Lu Songlin Du*

School of Automation, Southeast University, Nanjing, China

{luxiaoyong, sdu}@seu.edu.cn

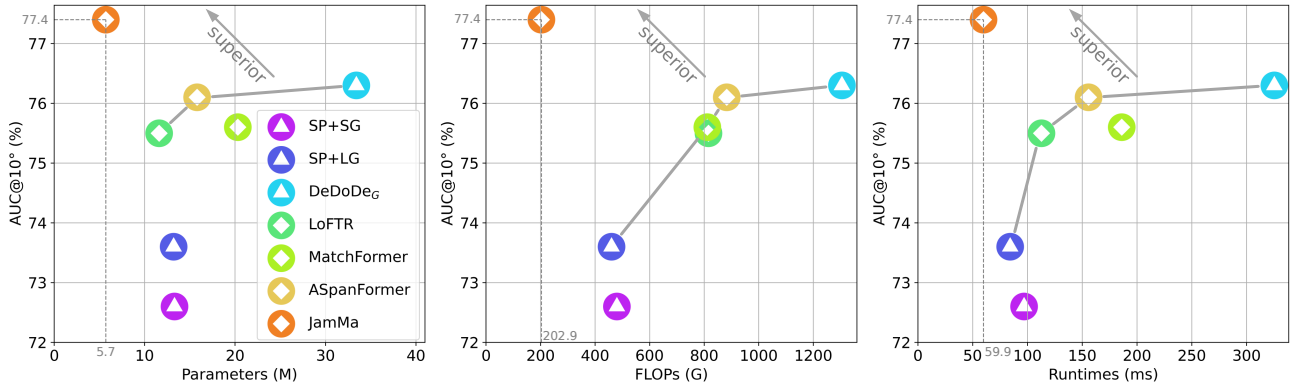


Figure 1. **Efficiency vs. Performance.** State-of-the-art sparse \blacktriangle and semi-dense \blacklozenge methods are compared in the MegaDepth dataset [19]. In all three commonly used efficiency metrics, the proposed JamMa achieves a superior performance-efficiency balance by a clear margin.

Abstract

Existing state-of-the-art feature matchers capture long-range dependencies with Transformers but are hindered by high spatial complexity, leading to demanding training and high-latency inference. Striking a better balance between performance and efficiency remains a challenge in feature matching. Inspired by the linear complexity $\mathcal{O}(N)$ of Mamba, we propose an ultra-lightweight Mamba-based matcher, named JamMa, which converges on a single GPU and achieves an impressive performance-efficiency balance in inference. To unlock the potential of Mamba for feature matching, we propose Joint Mamba with a scan-merge strategy named **JEGO**, which enables: (1) **J**oint scan of two images to achieve high-frequency mutual interaction, (2) **E**fficient scan with skip steps to reduce sequence length, (3) **G**lobal receptive field, and (4) **O**mnidirectional feature representation. With the above properties, the JEGO strategy significantly outperforms the scan-merge strategies proposed in VMamba and EVMamba in the feature matching task. Compared to attention-based sparse and semi-dense matchers, JamMa demonstrates a superior balance between performance and efficiency, delivering better performance with less than 50% of the parameters and FLOPs. Project page: <https://leoluxxx.github.io/JamMa-page/>.

*Corresponding author.

1. Introduction

Feature matching, which seeks to establish accurate correspondences between two images, underpins various critical tasks, including structure from motion (SfM) [34] and simultaneous localization and mapping (SLAM) [12]. However, feature matching faces challenges arising from variations in viewpoint, illumination, and scale. Furthermore, applications that demand real-time performance place significant pressure on the efficiency of the matching process.

Feature matching methods are generally classified into three categories: sparse, semi-dense, and dense methods. Sparse methods [4, 25, 33, 35], which operate alongside a keypoint detector [8, 23], are designed to establish correspondences between two sets of keypoints. Therefore, when the detector performs poorly in challenging scenes, such as texture-less scenes, it will severely affect the sparse matcher. In contrast, semi-dense and dense methods [5, 9, 11, 36] directly establish correspondences between grid points or all pixels, enhancing robustness in challenging scenes. However, semi-dense and dense matchers typically rely on Transformers [16, 40] to model long-range dependencies in dense features, resulting in impractically high complexity when processing high-resolution images. Achieving an optimal balance between performance and efficiency remains a critical challenge in feature matching.

To achieve high efficiency and robustness in challenging

Method	Omnidirectional	Global	Complexity
Transformer [40]	-	✓	N^2
EVMamba [27]	✗	✗	N
Vim [46]	✗	✓	$2N$
VMamba [21]	✓	✓	$4N$
JamMa	✓	✓	N

Table 1. **Model Property.** N denotes the number of features.

scenes, we explore the potential of accelerating semi-dense paradigm with Mamba, which captures long-range dependencies with linear complexity and has demonstrated significant success in natural language processing (NLP). However, since Mamba is originally designed as a sequence model for NLP, we identify three key challenges that hinder its suitability for feature matching and propose the Joint Mamba with JEGO strategy to address these issues efficiently:

(1) **Lack of Mutual Interaction.** Mamba is designed for modeling a single set of features, *i.e.*, *internal interaction*, whereas feature matching inherently requires interaction between two sets of features, *i.e.*, *mutual interaction*. Therefore, a new scan strategy is needed to effectively establish cross-view dependencies between two images. To this end, we explore two candidate strategies: joint scan and sequential scan, as shown in Fig. 4. Our findings indicate that joint scan, which alternates between the two images to facilitate *high-frequency mutual interaction*, significantly outperforms the sequential scan, in which each image is scanned individually and in sequence. Considering the necessity of mutual interaction for feature matching, the joint scan is adopted as a core component of the JEGO strategy, which also gives rise to the term Joint Mamba.

(2) **Unidirectionality.** Mamba is unidirectional as it generates sequences with a 1D forward scan. However, features exhibit relationships in four basic directions in 2D images, requiring the development of new scan strategies. As shown in Fig. 2, Vim [46] and VMamba [21] propose bi-directional and four-directional scans, respectively, but at the cost of a $2\times$ and $4\times$ increase in total sequence length. EVMamba [27] maintains a total sequence length equal to the original feature number N by skipping during scanning but fails to achieve omnidirectionality. The proposed JEGO strategy reconciles the skip scan with the four-directional scan, achieving both omnidirectionality and a total sequence length of N .

(3) **Causality.** Mamba operates as a causal model, allowing each feature in the sequence to perceive only the preceding features. As a result, only the end **E** of the sequence has access to the global receptive field. Numerous works have validated the importance of large receptive fields for visual models, including visual Mamba models. As shown in Fig. 2, Vim [46] and VMamba [21] achieve a global receptive field through backward scans (dashed lines), increasing the total sequence length to $2N$ and $4N$. EVMamba [27] maintains high efficiency but only forward-scans the sequence, which limits the global receptive field to only the bottom-right cor-

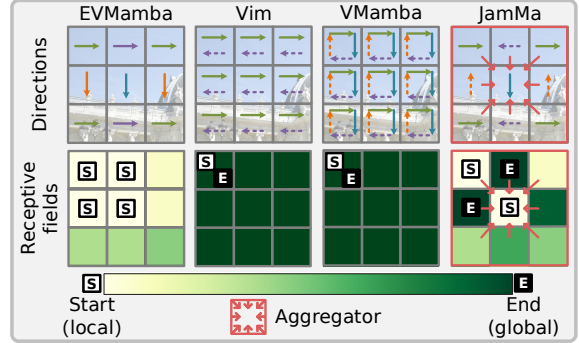


Figure 2. **Receptive Fields and Sequence Directions of Visual Mamba Models.**

ner. In the JEGO strategy, the scans in four directions are arranged to ensure a *balanced receptive field*, where *small receptive field features are consistently adjacent to those with larger ones* as shown in Fig. 2. A CNN termed aggregator is then employed to aggregate global information from four directions into features with small receptive fields. We find that a simple aggregator on a balanced receptive field has a surprisingly effective impact, intuitively ensuring that each feature is *global* and *omnidirectional*, see Fig. 6. To summarize, this paper presents the following contributions:

- We present JamMa, an ultra-lightweight semi-dense feature matcher based on Joint Mamba with JEGO strategy.
- A scan-merge strategy named **JEGO** is proposed, which **J**ointly scans cross-view features with high **E**fficiency and produces **G**lobal **O**mnidirectional features.
- High-frequency mutual interaction and a local aggregator on a balanced receptive field yield surprisingly robust features with minimal computational overhead.
- Quantitative and qualitative experiments demonstrate the excellent performance-efficiency balance of JamMa and highlight the critical role of the JEGO strategy.

2. Related Works

2.1. Local Feature Matching

Sparse matching encompasses well-known handcrafted methods such as SIFT [23], SURF [2], BRIEF [3], and ORB [31]. The rise of deep learning has shifted research focus toward learning-based methods. Models like R2D2 [29] and SuperPoint [8] employ convolutional neural networks (CNN) to improve robustness. SuperGlue [33] is the first to model global relationships between sparse features using Transformers [40], enriching features through self- and cross-attention. Recent attention-based sparse methods [4, 20, 25, 35] generally address the computational inefficiencies but still rely heavily on the performance of detector. **Semi-dense matching** methods are pioneered by LoFTR [36], which proposes a coarse-to-fine paradigm to establish coarse matches between grids and then adjust the matching points with fine features. ASpanFormer [5] proposes a new

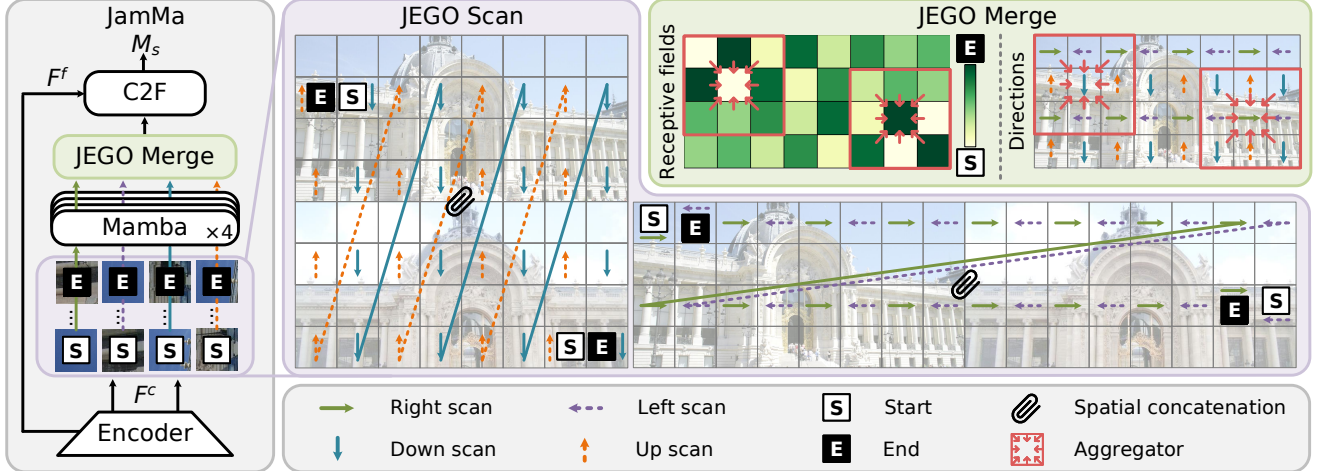


Figure 3. **Overview of the Proposed Method.** JamMa extracts coarse and fine local features with a CNN encoder (Sec. 3.2) and scans the coarse features with the JEGO scan module (Sec. 3.3.1). The four sequences are processed by four independent Mamba blocks and then merged back into 2D feature maps by the JEGO merge module (Sec. 3.3.2). Finally, the coarse-to-fine matching module (C2F) generates the matching results (Sec. 3.4). We show how the **JEGO** strategy enables **Joint, Efficient, Global, and Omnidirectional** scanning and merging.

alternative to linear attention [16] that adaptively adjusts the span of attention based on uncertainty. MatchFormer [41] abandons the CNN-based feature extractor and proposes a purely attention-based matcher to improve robustness. Semi-dense methods excel in texture-less scenes because they match grids distributed across the image. However, the large number of grid points also introduces a greater computational burden, particularly when matchers utilize attention mechanisms to establish long-distance dependencies.

Dense matching methods directly estimate dense warp to establish correspondence for each pixel between two images. Some approaches [7, 18, 30] utilize the 4D correlation volume to predict the dense warp. Recently, DKM [9] and RoMa [11] have introduced a kernelized global matcher and an embedding decoder to initially predict coarse warps, which are subsequently refined using stacked feature maps. While DKM and RoMa outperform sparse and semi-dense methods in terms of accuracy and robustness, they demand significantly more parameters and longer runtimes.

2.2. State Space Models

State Space Models (SSM) are initially designed to model continuous linear time-invariant systems [43], where an input signal $x(t)$ is mapped to its output signal $y(t)$ as

$$h'(t) = Ah(t) + Bx(t), \quad y(t) = Ch'(t). \quad (1)$$

$A \in \mathbb{R}^{N \times N}$, $B \in \mathbb{R}^{N \times 1}$ and $C \in \mathbb{R}^{1 \times N}$ are SSM parameters. To adapt SSM in discrete systems, *e.g.*, sequence-to-sequence tasks, S4 [15] proposes to transform SSM parameters to their discretized counterparts using the zero-order hold rule. However, S4 shares parameters across all time steps, which severely limits its representational capacity. Mamba [14] proposes S6 which makes SSM parameters de-

pendent on the input sequence. This data-dependent property significantly enhances Mamba, making its performance comparable to Transformer. Meanwhile, the primary reason for the high efficiency of Mamba is that the repetitive computations in SSM can be performed once by a global convolution kernel, which can be pre-computed via the SSM parameters.

Following the success of Mamba, there has been a surge in applying the framework to computer vision tasks. Visual Mamba models generally scan 2D feature maps into 1D sequences to model them with Mamba and then merge the 1D sequences back to 2D feature maps. Vim [46] and VMamba [21] propose the bi-directional scan and four-directional scan, respectively, extending the originally causal Mamba to achieve a global receptive field. EVMamba [27] proposes the skip scan to reduce the sequence length thereby significantly improving efficiency. The above visual Mamba models focus on single-image tasks, *e.g.*, image classification. In contrast, we propose Joint Mamba, which is designed to jointly model *two images* for feature matching.

3. Methodology

3.1. JamMa Overview

The overall architecture of JamMa is illustrated in Fig. 3. We extract the coarse features F^c and fine features F^f with a CNN encoder. The coarse features are then processed by Joint Mamba, *i.e.*, JEGO scan \rightarrow Mamba \rightarrow JEGO merge, to perform internal and mutual interaction, perceiving global and omnidirectional information of two images. Finally, we utilize the coarse-to-fine matching (C2F) module to generate matching results. Specifically, we establish bi-directional coarse matches and adjust coarse match points in fine matching and sub-pixel refinement modules [38].

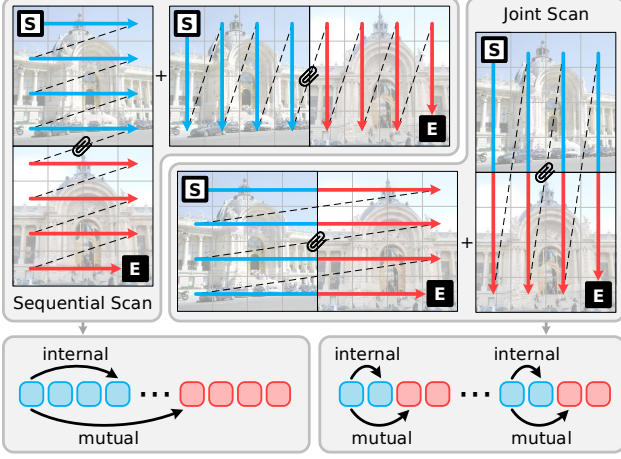


Figure 4. **Sequential scan vs. Joint scan.** Sequential scan follows a pattern of internal \rightarrow mutual interaction, similar to self \rightarrow cross attention. Joint scan, by contrast, emphasizes high-frequency mutual interaction, which has proven crucial for feature matching.

3.2. Local Feature Extraction

We adopt the ConvNeXt V2 [44] as the encoder to extract local coarse features $F^c \in \mathbb{R}^{H_c \times W_c \times C_1}$ and fine features $F^f \in \mathbb{R}^{H_f \times W_f \times C_2}$ from images I_A and I_B as

$$F_A^c, F_A^f = \text{Encoder}(I_A), \quad F_B^c, F_B^f = \text{Encoder}(I_B). \quad (2)$$

We observe that the designs of ConvNeXt perform remarkably well in lightweight settings. Specifically, a ConvNeXt-based encoder with 0.65M parameters is sufficient to support JamMa for competitive performance.

3.3. Joint Mamba

Joint Mamba, comprising JEGO scan, Mamba, and JEGO merge, is proposed to efficiently establish global dependencies in coarse features $F_{A,B}^c$ for robust coarse matching.

3.3.1 JEGO Scan

Joint Scan. Existing Mamba models are designed for single-image tasks, whereas feature matching requires interaction between two sets of features. Attention-based matchers, for example, utilize self- and cross-attention for internal and mutual interaction. Therefore, a new scan strategy is needed to achieve both internal and mutual interaction.

We begin by concatenating the coarse features $F_{A,B}^c$ both horizontally and vertically as

$$X^h = [F_A^c | F_B^c], \quad X^v = \begin{bmatrix} F_A^c \\ F_B^c \end{bmatrix}. \quad (3)$$

Based on X^h and X^v , we explore two candidate scan strategies: sequential scan and joint scan, as shown in Fig. 4. In the sequential scan, all features of one image are scanned before moving to the next. In contrast, the joint scan alternates between the two images to enable high-frequency

mutual interaction, which is beneficial for cross-view dependencies. We show in Tab. 4 that the joint scan is significantly more effective for feature matching than the sequential scan. **Efficient Four-directional Scan.** In addition to the proposed joint scan, the JEGO scan also incorporates the skip scan strategy introduced in EVMamba [27], which scans features at intervals rather than exhaustively to reduce the sequence length. However, EVMamba only performs forward scans, resulting in a global receptive field restricted to the bottom-right of the image and lacking omnidirectionality. By arranging the starting points \mathbf{S} and ending points \mathbf{E} of the sequences in four directions as in Fig. 2, the JEGO scan achieves a balanced receptive field and omnidirectionality.

Four sequences $\{S_i\}_{i=1}^4$ of length $N/4$ in four directions are generated through horizontal scan on X^h and vertical scan on X^v . $S_1, S_2, S_3, S_4 \in \mathbb{R}^{2H_c W_c / p^2 \times C_1}$ represent the sequences of right, left, up, and down scans, respectively. These sequences are then processed independently by four Mamba blocks to establish long-range dependencies.

$$\begin{aligned} S_{1,2} &\stackrel{\text{horizontal scan}}{\leftarrow} X^h[m :: p, n :: p, :], \\ S_{3,4} &\stackrel{\text{vertical scan}}{\leftarrow} X^v[m :: p, n :: p, :], \\ S_{2,4} &= \text{Flip}(S_{2,4}), \\ \{\tilde{S}_i\}_{i=1}^4 &= \text{Mamba}(\{S_i\}_{i=1}^4), \end{aligned} \quad (4)$$

where the operation $[m :: p, n :: p, :]$ denotes slicing the matrix for each channel, starting at m in height and n in width, while skipping every $p = 2$ steps. The starting point \mathbf{S} (m, n) for each sequence is arranged as

$$(m, n) = \left(\left\lfloor \frac{i-1}{2} \right\rfloor, (i-1) \bmod 2 \right), \quad i \in \{1, 2, 3, 4\}. \quad (5)$$

3.3.2 JEGO Merge

After establishing long-range dependencies in each sequence individually, merging the sequences into a 2D feature map is crucial for visual tasks. To address this, we propose the JEGO merge strategy to produce global omnidirectional feature maps for two images.

First, we restore the features in four sequences to their original scanned positions, resulting in the joint feature maps $Y^h \in \mathbb{R}^{2H_c \times W_c \times C_1}$ and $Y^v \in \mathbb{R}^{H_c \times 2W_c \times C_1}$,

$$\begin{aligned} \tilde{S}_{2,4} &= \text{Flip}(\tilde{S}_{2,4}), \\ Y^h[m :: p, n :: p, :] &\stackrel{\text{restore}}{\leftarrow} \tilde{S}_{1,2}, \\ Y^v[m :: p, n :: p, :] &\stackrel{\text{restore}}{\leftarrow} \tilde{S}_{3,4}. \end{aligned} \quad (6)$$

Then we spatially split the joint feature maps Y^h and Y^v into the features of image I_A and I_B , e.g., $Y^h \rightarrow Y_A^h, Y_B^h$. The horizontal and vertical features are summed to obtain the merged feature maps $\tilde{F}_A^c, \tilde{F}_B^c \in \mathbb{R}^{H_c \times W_c \times C_1}$ as

$$\begin{aligned} \tilde{F}_A^c &= Y_A^h + Y_A^v = Y_h[:, H_c, :, :] + Y_v[:, :, W_c, :], \\ \tilde{F}_B^c &= Y_B^h + Y_B^v = Y_h[H_c, :, :, :] + Y_v[:, :, W_c, :, :]. \end{aligned} \quad (7)$$

Although \hat{F}_A^c, \hat{F}_B^c are omnidirectional and exhibit balanced receptive fields at the macro level, each individual feature still perceives unidirectional information and has local receptive fields at the micro level, except at the ends **E** of the four sequences. Therefore, we propose using a gated convolutional unit as an aggregator for local information aggregation in 3×3 windows, consolidating information from *different directions and receptive fields* toward the center as

$$\begin{aligned} \sigma &= \text{GELU}(\text{Conv}_3(\tilde{F}^c)), \\ \hat{F}^c &= \text{Conv}_3(\sigma \cdot \text{Conv}_3(\tilde{F}^c)). \end{aligned} \quad (8)$$

Conv_3 denote 2D convolutions with a kernel size of 3, and σ is the gating signal that determines which information is filtered based on the input. The aggregator ensures that \hat{F}_A^c and \hat{F}_B^c are *global* and *omnidirectional* at the micro level, which is essential to the performance of JamMa.

3.4. Coarse-to-Fine Matching

Based on the aggregated coarse features $\hat{F}_{A,B}^c$ and the fine features $F_{A,B}^f$, we adopt the coarse-to-fine matching module in XoFTR [38] to generate matches, as shown in Fig. 5.

Coarse Matching. The coarse similarity matrix S_c between two sets of coarse features is computed as

$$S_c(i, j) = \frac{1}{\tau} \cdot \langle \hat{F}_A^c(i), \hat{F}_B^c(j) \rangle, \quad (9)$$

where τ is a temperature parameter and $\langle \cdot, \cdot \rangle$ denotes the inner product. We then perform row Softmax_{row} and column Softmax_{col} separately on the similarity matrix to obtain matching probability matrices $P_{A \rightarrow B}$ and $P_{B \rightarrow A}$ as

$$\begin{aligned} P_{A \rightarrow B} &= \text{Softmax}_{row}(S_c), \\ P_{B \rightarrow A} &= \text{Softmax}_{col}(S_c). \end{aligned} \quad (10)$$

We can assign \hat{F}_A^c to \hat{F}_B^c via $P_{A \rightarrow B}$ in a many-to-one fashion [24], and similarly assign \hat{F}_B^c to \hat{F}_A^c via $P_{B \rightarrow A}$, resulting in two sets of matches $M_{A \rightarrow B}$ and $M_{B \rightarrow A}$. Specifically, we establish $M_{A \rightarrow B}$ and $M_{B \rightarrow A}$ following two criteria: (1) row-maximum in $P_{A \rightarrow B}$ or column-maximum in $P_{B \rightarrow A}$, and (2) confidences greater than the threshold θ_c . The union of $M_{A \rightarrow B}$ and $M_{B \rightarrow A}$ is then considered as the coarse matches M_c , which is more robust than one-to-one matches obtained through Dual-Softmax operation.

$$\begin{aligned} M_c &= \{(i, j) \mid P_{i,j}^{A \rightarrow B} = \max_k \mathcal{P}_{i,k}^{A \rightarrow B}, P_{i,j}^{A \rightarrow B} \geq \theta_c\} \\ &\cup \{(i, j) \mid P_{i,j}^{B \rightarrow A} = \max_k \mathcal{P}_{k,j}^{B \rightarrow A}, P_{i,j}^{B \rightarrow A} \geq \theta_c\}. \end{aligned} \quad (11)$$

Fine Matching. For each coarse match, two 5×5 feature windows $\hat{F}_A^f, \hat{F}_B^f \in \mathbb{R}^{M \times 25 \times C_2}$ are cropped from the fine features F_A^f, F_B^f , where M is the number of coarse matches. \hat{F}_A^f and \hat{F}_B^f are then processed by the MLP-Mixer [37] to

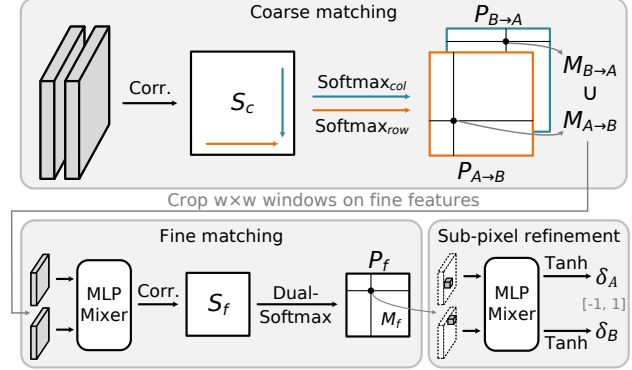


Figure 5. **Coarse-to-Fine Matching (C2F) Module.**

enable mutual interaction in a lightweight manner. Similar to Eq. (9), the fine similarity matrix $S_f \in \mathbb{R}^{M \times 25 \times 25}$ is computed by the inner product, and the Dual-Softmax is applied to calculate fine matching probability matrix P_f as

$$P_f = \text{Softmax}_{row}(S_f) \cdot \text{Softmax}_{col}(S_f). \quad (12)$$

We further apply the mutual nearest neighbor (MNN) criteria to establish one-to-one fine matches M_f .

Sub-pixel Refinement. Since classification-based matches M_f cannot achieve sub-pixel accuracy, regression-based refinement is employed to further adjust the matches. For each fine match, $F_A^s, F_B^s \in \mathbb{R}^{M \times 1 \times C_2}$ are cropped from the feature windows, which are then processed by the MLP-Mixer. The Tanh activation function is used to compute offsets $\delta_A, \delta_B \in [-1, 1]^{M \times 2}$, which are then added to M_f for adjustment, resulting in final sub-pixel matches M_s .

3.5. Supervision

Our loss function comprises three components: the coarse matching loss \mathcal{L}_c , the fine matching loss \mathcal{L}_f , and the sub-pixel loss \mathcal{L}_s . The ground-truth matching matrices P_c^{gt} and P_f^{gt} are generated from the camera poses and depth maps.

The coarse matching loss \mathcal{L}_c is computed as the focal loss FL between P_c^{gt} and $P_{A \rightarrow B}, P_{B \rightarrow A}$,

$$\mathcal{L}_c = \text{FL}(P_c^{gt}, P_{A \rightarrow B}) + \text{FL}(P_c^{gt}, P_{B \rightarrow A}). \quad (13)$$

The fine matching loss \mathcal{L}_f is computed as the focal loss between P_f^{gt} and P_f ,

$$\mathcal{L}_f = \text{FL}(P_f^{gt}, P_f). \quad (14)$$

In line with XoFTR [38], we implement the symmetric epipolar distance function to compute the sub-pixel refinement loss as

$$\mathcal{L}_s = \frac{1}{|M_f|} \sum_{(x,y)} \|x^T E y\|^2 \left(\frac{1}{\|E^T x\|_{0.2}^2} + \frac{1}{\|E y\|_{0.2}^2} \right), \quad (15)$$

where x and y are the homogeneous coordinates of matching points M_s , and E denotes the ground-truth essential matrix.

Category	Method	Avg. Rank ↓	Efficiency ↓			Relative Pose Estimation ↑		
			Params (M)	FLOPs (G)	Time (ms)	AUC@5°	AUC@10°	AUC@20°
Sparse	XFeat [28]	7.5	0.7	15.7	14.2	44.2	58.2	69.2
	SP [8] + SG [33]	9.2	13.3	480.2	96.9	57.6	72.6	83.5
	SP [8] + LG [20]	7.3	13.2	459.9	84.2	58.8	73.6	84.1
	DeDoDe _B [10]	10.7	28.1	1268.2	189.1	61.1	73.8	83.0
	DeDoDe _G [10]	8.5	33.4	1304.8	329.5	62.8	76.3	85.8
Dense	DKM [9]	7.5	72.3	1424.5	554.2	67.3	79.7	88.1
	RoMa [11]	7.5	111.3	2014.3	824.9	68.5	80.6	88.8
Semi-Dense	XFeat* [28]	7.5	1.5	48.4	29.0	50.8	66.8	78.8
	RCM [24]	7.5	9.8	363.6	93.0	58.3	72.8	83.5
	LoFTR [36]	7.3	11.6	815.4	117.5	62.1	75.5	84.9
	MatchFormer [41]	8.3	20.3	811.1	186.0	62.0	75.6	84.9
	ASpanFormer [5]	7.3	15.8	882.3	155.7	62.6	76.1	85.7
	ELoFTR [42]	5.8	16.0	968.8	69.6	63.7	77.0	86.4
	JamMa	3	5.7	202.9	59.9	64.1	77.4	86.5

Table 2. **Results of Relative Pose Estimation on MegaDepth [19] Dataset.** The AUC of pose error at three thresholds and the overall efficiency of models are presented. To indicate the performance-efficiency balance, we report the average ranking across six metrics of efficiency and relative pose estimation. The 1st, 2nd, and 3rd -best methods are highlighted.

4. Experiments

4.1. Implementation Details

The proposed method is implemented using Pytorch [26]. For feature extraction, we adopt the first two stages of ConvNeXt V2-N, which contains 0.65M parameters. JamMa comprises 4 Mamba blocks that process sequences in four directions. The channel dimensions for the coarse and fine features are $C_1 = 256$ and $C_2 = 64$, respectively. The coarse feature resolution is $1/8$, and the fine feature resolution is $1/2$. The temperature parameter τ is set to 0.1, and the coarse matching threshold θ_c is set to 0.2. JamMa is trained on the MegaDepth dataset [19] for 30 epochs with a batch size of 2 using the AdamW optimizer [22], and it is not fine-tuned for any other tasks. During training, images are resized and padded to a size of 832×832 . The initial learning rate is set to 0.0002, and a cosine decay learning rate scheduler with 1 epoch of linear warm-up is employed. Network training takes ~ 50 hours on a single NVIDIA 4090 GPU, and all evaluations are also conducted on this GPU.

4.2. Relative Pose Estimation

Dataset. We evaluate matchers on the MegaDepth dataset [19] for pose estimation. Test images are resized and padded to 832×832 , the same as the training size. As suggested in [20], we use LO-RANSAC [17] to estimate essential matrix for all methods, as it is more robust than vanilla RANSAC, enhancing evaluation reliability. The detailed evaluation setup of each method is reported in the Appendix.

Metric. The area under the cumulative curve (AUC) of the pose error at thresholds (5° , 10° , 20°) are reported. We also report three efficiency metrics including parameters, FLOPs, and runtime, along with the average ranking across six metrics of efficiency and performance.

Category	Method	Homography est. AUC		
		@3px	@5px	@10px
Sparse	SP [8] + NN	41.6	55.8	71.7
	R2D2 [29] + NN	50.6	63.9	76.8
	DISK [39] + NN	52.3	64.9	78.9
	SP [8] + SG [33]	53.9	68.3	81.7
	SP [8] + LG [20]	54.2	68.3	81.5
Semi-Dense	DRC-Net [18]	50.6	56.2	68.3
	LoFTR [36]	65.9	75.6	84.6
	ASpanFormer [5]	67.4	76.9	85.6
	ELoFTR [42]	66.5	76.4	85.5
	JamMa	68.1	77.0	85.4

Table 3. **Results of Homography Estimation on HPatches [1] Dataset.** The AUC of reprojection error of corner points at different thresholds are reported.

Results. With 14 evaluated methods, an average ranking of 7.5 is defined as the expected performance-efficiency balance, *e.g.*, the best performance with the worst efficiency. As presented in Tab. 2, JamMa achieves an average ranking of 3.5, leading the expected balance and other matchers by a large margin. In terms of performance, JamMa demonstrates the best pose estimation results among evaluated semi-dense and sparse matchers, surpassed only by the dense matchers DKM and RoMa that prioritize accuracy. In terms of efficiency, JamMa exceeds all evaluated matchers except XFeat and XFeat*. JamMa has notably fewer parameters than attention-based matchers, making it ultra-lightweight.

4.3. Homography Estimation

Dataset. The HPatches dataset [1] contains planar scenes for evaluating homography estimation. We assess the performance of our method across 108 HPatches sequences, which comprise 52 sequences with illumination variations and 56 sequences with viewpoint changes.

Metric. Following the evaluation protocol proposed in

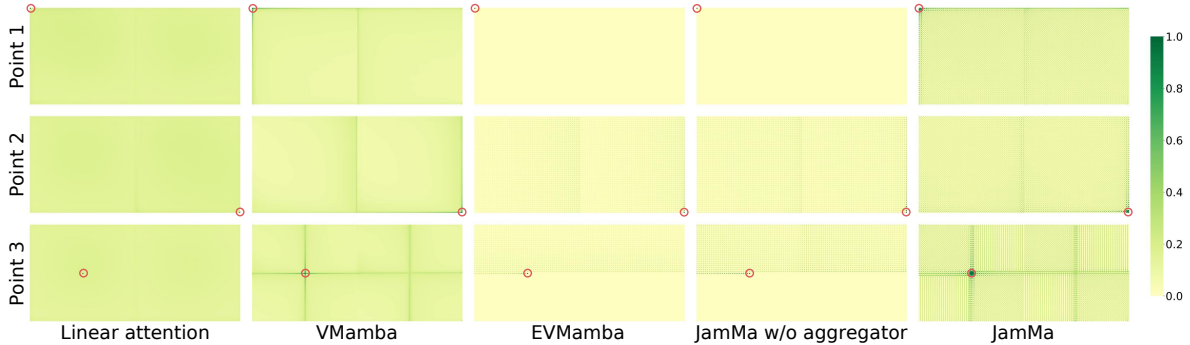


Figure 6. **Effective Receptive Field (ERF)**. Red circles denote query points, and the ERFs of query points in the two images are concatenated horizontally. JamMa achieves a global and omnidirectional receptive field, a capability made possible through the aggregator.

Method	Time* (ms)	Pose est. AUC		
		@5°	@10°	@20°
JamMa	3.2	64.5	77.3	86.3
(1) Replace JS to SS	3.2	62.2	74.7	83.7
(2) w/o Aggregator	3.0	62.3	75.1	84.3
(3) w/ EVMamba scan	3.0	61.9	74.8	84.1
(4) w/ VMamba scan	9.7	64.1	77.1	86.2
(5) w/ van. attention		OOM		
(6) w/ lin. attention	24.3	64.2	77.0	86.1
(7) w/o interaction	0	60.1	73.0	82.6

Table 4. **Ablation Study**. SS and JS denote sequential scan and joint scan, respectively. The superscript * indicates that the time of the coarse layer, including scanning and merging, is reported.

LoFTR [36], we compute the mean reprojection error of corner points, and report the AUC of the corner error up to threshold values of 3, 5, and 10 pixels, respectively. All images are resized so that their smaller dimension is equal to 480 pixels. Vanilla RANSAC [13] is applied to estimate the homography for all methods. The top 1000 matches of semi-dense methods are selected for the sake of fairness.

Results. As shown in Tab. 3, JamMa achieves competitive performance in homography estimation. Comparing the state-of-the-art matcher ASpanFormer, JamMa lags behind by 0.2% at threshold 10 but leads by 0.7% at threshold 3. It is worth noting that JamMa is much more lightweight than ASpanFormer, with only 36% of its parameters. We attribute this favorable performance-efficiency balance to the global omnidirectional representation resulting from the JEGO strategy and the Mamba with linear complexity.

4.4. Ablation Study

We conduct qualitative and quantitative ablation studies on the MegaDepth dataset for a comprehensive understanding of JamMa. Models in Tab. 4 are trained for 15 epochs at 544 resolution and tested with the same settings as in Sec. 4.2.

Joint Scan. As shown in Tab. 4(1), replacing the joint scan with the sequential scan leads to a significant performance drop of (-2.3%, -2.6%, -2.6%), which suggests that the joint scan is more effective for feature matching, as it promotes high-frequency mutual interactions between the two

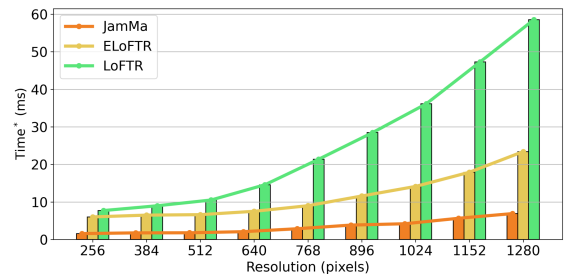


Figure 7. **Comparison of Coarse Layer Processing Times**.

images. Note that VMamba and EVMamba inherently lack mutual interaction capabilities, and thus, we introduce the joint scan to both methods for ablation studies (3) and (4).

Aggregator. We present the effective receptive fields (ERF) in Fig. 6, where the coarse features of JamMa achieve global receptive fields and perceive information from all directions. Without the aggregator, JamMa loses the global receptive field and omnidirectionality as previously analyzed. The results in Tab. 4(2) indicate a severe performance decline of (-2.2%, -2.2%, -2%) without the aggregator. More ablation studies of the aggregator are reported in the Appendix. Additionally, the comparison between (2) and (3) confirms that the four-directional scan outperforms the bi-directional scan in EVMamba, even in the absence of the aggregator.

Comparison with Mamba-based Methods. As shown in Tab. 4(3)(4), we evaluate the JEGO strategy against those proposed in EVMamba and VMamba. Compared to EVMamba, JamMa exhibits a substantial performance improvement of (+2.6%, +2.5%, +2.2%). While VMamba achieves a global receptive field as shown in Fig. 6, this comes at the cost of 4× total sequence length. Leveraging the JEGO strategy, JamMa layer achieves 3× speedup over the VMamba layer while delivering superior performance, resulting in a 9.5% overall speed improvement (68.3ms vs. 61.8ms).

Comparison with Attention-based Methods. In the case of (5) vanilla attention, the out-of-memory (OOM) error occurs in 24GB VRAM. Comparing (6) linear attention, JamMa achieves a performance boost of (+0.3%, +0.3%, +0.2%) while being 7.6× faster. JamMa minimizes the bottleneck of most matchers, *i.e.*, attention-based interaction, to nearly

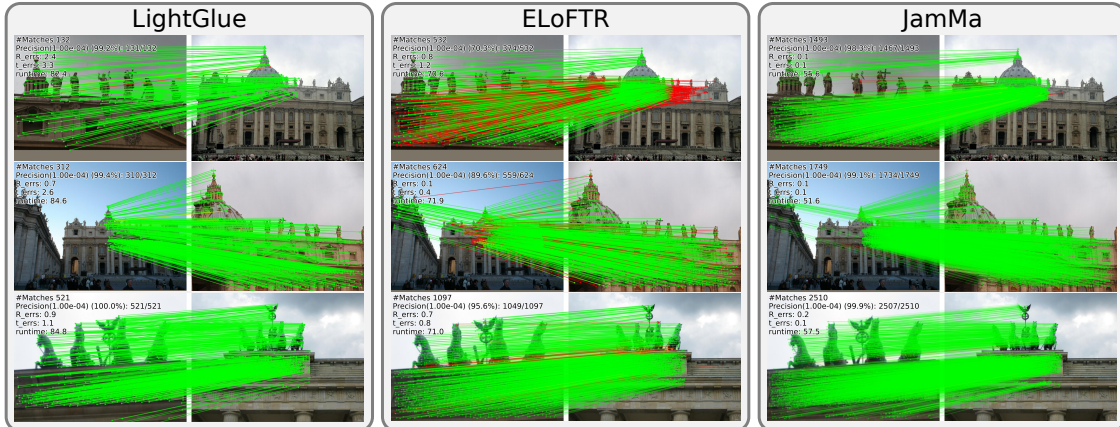


Figure 8. **Comparison of Qualitative Results.** The reported metrics include precision with an epipolar error threshold of 1×10^{-4} , rotation and translation errors in pose estimation, and runtime. JamMa consistently delivers more robust matching results with shorter runtime.

Method	Params (M)	Time (ms)	Pose est. AUC		
			@5°	@10°	@20°
JamMa	5.7	61.8	64.5	77.3	86.3
w/ XFeat	5.7	54.6	61.1	74.6	84.1
w/ SuperPoint	6.0	67.5	61.8	75.1	84.8
w/ ResNet	8.8	72.0	63.8	76.8	85.9

Table 5. **Ablation Studies on Encoder and Interaction.**

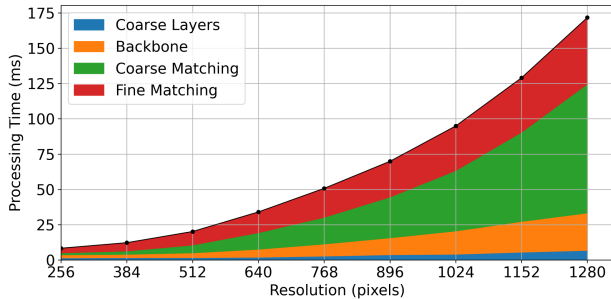


Figure 9. **Component Analysis of Runtime.**

negligible levels, significantly enhancing overall efficiency. The total runtimes of JamMa and (6) are 82.9ms vs. 61.8ms (a 25% total speed gain), and 4 JamMa layers and 4 linear attention layers contain parameters of 1.8M vs. 5.3M (a 66% parameter reduction). Fig. 7 further shows the processing time of coarse layers at various resolutions.

Encoders. The variants of JamMa, employing XFeat, SuperPoint, and ResNet as encoders, are shown in Tab. 5. JamMa delivers competitive results with different encoders, with ConvNeXt offering the best performance-efficiency balance.

5. Discussion

As shown in Fig. 9, we conduct a component analysis on the runtime of JamMa for further acceleration. Our findings indicate that, when processing coarse features with Joint Mamba, the coarse layers are no longer the efficiency bottleneck as observed in attention-based methods. Instead, coarse matching using Softmax on the large similarity matrix has

Method	Avg. Rank	Params (M)	Time (ms)	Pose est. AUC		
				@5°	@10°	@20°
SP [8]+SG [33]	3.6	13.3	35.8	16.5	32.2	48.8
SP [8]+LG [20]	2.6	13.2	22.9	15.9	32.2	49.7
LoFTR [36]	1.8	11.6	49.2	20.7	37.7	53.4
JamMa	1.8	5.7	26.6	18.5	35.6	51.3

Table 6. **Relative Pose Estimation on ScanNet [6] Dataset.**

emerged as new bottleneck that require optimization. We explore the Softmax-free coarse matching proposed in [42] and observe a 10ms speedup without a performance drop. Note that this optimization is excluded in Sec. 4 for fairness.

As shown in Tab. 6, we conduct zero-shot pose estimation experiments in the ScanNet [6] dataset. While JamMa achieves competitive performance in outdoor scenes, this does not fully transfer to indoor scenes, which we attribute to its reduced number of parameters (less than 50% of those in compared methods), potentially limiting the generalizability. Note that JamMa still strikes a reasonable performance-efficiency balance compared to other methods.

6. Conclusion

This paper presents JamMa, an ultra-lightweight Mamba-based feature matcher with competitive performance. We explore various scan-merge strategies for image pairs, a topic not previously investigated, as existing visual Mamba models focus on single-image tasks. Firstly, we find that joint scan with high-frequency mutual interaction substantially outperforms sequential scan, which resembles self- and cross-attention. Secondly, a four-directional scan is combined with an aggregator to generate global and omnidirectional features, which play a crucial role in performance. Thirdly, Mamba coupled with skip scan makes JamMa extremely efficient and even surpasses most attention-based sparse methods. Experiments demonstrate that JamMa achieves a remarkable balance between performance and efficiency.

References

- [1] V. Balntas, K. Lenc, A. Vedaldi, and K. Mikolajczyk. Hpatches: A benchmark and evaluation of handcrafted and learned local descriptors. In *Proceedings of the CVPR*, pages 5173–5182, 2017. 6
- [2] H. Bay, T. Tuytelaars, and L. Van G. SURF: Speeded Up Robust Features. In *Proceedings of the ECCV*, pages 404–417, 2006. 2
- [3] M. Calonder, V. Lepetit, C. Strecha, and P. Fua. BRIEF: Binary Robust Independent Elementary Features. In *Proceedings of the ECCV*, pages 778–792, 2010. 2
- [4] H. Chen, Z. Luo, J. Zhang, L. Zhou, X. Bai, Z. Hu, C. Tai, and L. Quan. Learning to match features with seeded graph matching network. In *Proceedings of the ICCV*, pages 6301–6310, 2021. 1, 2
- [5] H. Chen, Z. Luo, L. Zhou, Y. Tian, M. Zhen, T. Fang, D. McKinnon, Y. Tsin, and L. Quan. Aspanformer: Detector-free image matching with adaptive span transformer. In *Proceedings of the ECCV*, pages 20–36, 2022. 1, 2, 6, 3
- [6] A. Dai, A. X Chang, M. Savva, M. Halber, T. Funkhouser, and M. Nießner. Scannet: Richly-annotated 3d reconstructions of indoor scenes. In *Proceedings of the CVPR*, pages 5828–5839, 2017. 8
- [7] F. Darmon, M. Aubry, and P. Monasse. Learning to guide local feature matches. In *Proceedings of the 3DV*, pages 1127–1136, 2020. 3
- [8] D. DeTone, T. Malisiewicz, and A. Rabinovich. SuperPoint: Self-Supervised Interest Point Detection and Description. In *Proceedings of the CVPRW*, pages 224–236, 2018. 1, 2, 6, 8, 3
- [9] Johan Edstedt, Ioannis Athanasiadis, Mårten Wadenbäck, and Michael Felsberg. Dkm: Dense kernelized feature matching for geometry estimation. In *Proceedings of the CVPR*, pages 17765–17775, 2023. 1, 3, 6
- [10] Johan Edstedt, Georg Bökman, Mårten Wadenbäck, and Michael Felsberg. Dedode: Detect, don’t describe—describe, don’t detect for local feature matching. In *Proceedings of the 3DV*, pages 148–157, 2024. 6, 3
- [11] Johan Edstedt, Qiyu Sun, Georg Bökman, Mårten Wadenbäck, and Michael Felsberg. Roma: Robust dense feature matching. In *Proceedings of the CVPR*, pages 19790–19800, 2024. 1, 3, 6
- [12] J. Engel, V. Koltun, and D. Cremers. Direct sparse odometry. *IEEE Transactions on Pattern Analysis and Machine Intelligence*, 40(3):611–625, 2017. 1
- [13] M. A Fischler and R. C Bolles. Random sample consensus: a paradigm for model fitting with applications to image analysis and automated cartography. *Communications of the ACM*, pages 381–395, 1981. 7
- [14] Albert Gu and Tri Dao. Mamba: Linear-time sequence modeling with selective state spaces, 2024. 3, 1
- [15] Albert Gu, Karan Goel, and Christopher Ré. Efficiently modeling long sequences with structured state spaces. *arXiv preprint arXiv:2111.00396*, 2021. 3
- [16] A. Katharopoulos, A. Vyas, N. Pappas, and F. Fleuret. Transformers are rnns: Fast autoregressive transformers with linear attention. In *Proceedings of the ICML*, pages 5156–5165, 2020. 1, 3
- [17] Viktor Larsson. Poselib-minimal solvers for camera pose estimation, 2020. 6
- [18] X. Li, K. Han, S. Li, and V. Prisacariu. Dual-resolution correspondence networks. In *Proceedings of the NeurIPS*, pages 17346–17357, 2020. 3, 6
- [19] Z. Li and N. Snavely. MegaDepth: Learning Single-View Depth Prediction from Internet Photos. In *Proceedings of the CVPR*, pages 2041–2050, 2018. 1, 6
- [20] P. Lindenberger, P. Sarlin, and M. Pollefeys. Lightglue: Local feature matching at light speed. In *Proceedings of the ICCV*, pages 17627–17638, 2023. 2, 6, 8, 3
- [21] Yue Liu, Yunjie Tian, Yuzhong Zhao, Hongtian Yu, Lingxi Xie, Yaowei Wang, Qixiang Ye, and Yunfan Liu. Vmamba: Visual state space model. *arXiv preprint arXiv:2401.10166*, 2024. 2, 3
- [22] I. Loshchilov and F. Hutter. Decoupled weight decay regularization. *arXiv preprint arXiv:1711.05101*, 2017. 6
- [23] D. G. Lowe. Distinctive Image Features from Scale-Invariant Keypoints. *International Journal of Computer Vision*, 60(2): 91–110, 2004. 1, 2
- [24] Xiaoyong Lu and Songlin Du. Raising the ceiling: Conflict-free local feature matching with dynamic view switching. In *Proceedings of the ECCV*, pages 256–273, 2025. 5, 6
- [25] X. Lu, Y. Yan, B. Kang, and S. Du. Paraformer: Parallel attention transformer for efficient feature matching. *arXiv preprint arXiv:2303.00941*, 2023. 1, 2
- [26] A. Paszke, S. Gross, F. Massa, A. Lerer, J. Bradbury, G. Chanan, T. Killeen, Z. Lin, N. Gimelshein, L. Antiga, et al. Pytorch: An imperative style, high-performance deep learning library. *Proceedings of the NeurIPS*, 32, 2019. 6
- [27] Xiaohuan Pei, Tao Huang, and Chang Xu. Efficientvmamba: Atrous selective scan for light weight visual mamba. *arXiv preprint arXiv:2403.09977*, 2024. 2, 3, 4
- [28] Guilherme Potje, Felipe Cadar, André Araujo, Renato Martins, and Erickson R Nascimento. Xfeat: Accelerated features for lightweight image matching. In *Proceedings of the CVPR*, pages 2682–2691, 2024. 6
- [29] J. Revaud, C. De Souza, M. Humenberger, and P. Weinzaepfel. R2D2: Reliable and Repeatable Detector and Descriptor. In *Proceedings of the NeurIPS*, pages 12414–12424, 2019. 2, 6
- [30] I. Rocco, M. Cimpoi, R. Arandjelović, A. Torii, T. Pajdla, and J. Sivic. Neighbourhood consensus networks. In *Proceedings of the NeurIPS*, pages 1658–1669, 2018. 3
- [31] E. Rublee, V. Rabaud, K. Konolige, and G. Bradski. ORB: An efficient alternative to SIFT or SURF. In *Proceedings of the ICCV*, pages 2564–2571, 2011. 2
- [32] P. Sarlin, R. Cadena, C. and Siegwart, and M. Dymczyk. From coarse to fine: Robust hierarchical localization at large scale. In *Proceedings of the CVPR*, pages 12716–12725, 2019. 3
- [33] P. Sarlin, D. DeTone, T. Malisiewicz, and A. Rabinovich. SuperGlue: Learning Feature Matching With Graph Neural Networks. In *Proceedings of the CVPR*, pages 4937–4946, 2020. 1, 2, 6, 8
- [34] J. L. Schonberger and J. Frahm. Structure-from-motion revisited. In *Proceedings of the CVPR*, pages 4104–4113, 2016. 1

- [35] Y. Shi, J. Cai, Y. Shavit, T. Mu, W. Feng, and K. Zhang. Clustergnn: Cluster-based coarse-to-fine graph neural network for efficient feature matching. In *Proceedings of the CVPR*, pages 12517–12526, 2022. [1](#), [2](#)
- [36] J. Sun, Z. Shen, Y. Wang, H. Bao, and X. Zhou. LoFTR: Detector-Free Local Feature Matching With Transformers. In *Proceedings of the CVPR*, pages 8922–8931, 2021. [1](#), [2](#), [6](#), [7](#), [8](#), [3](#)
- [37] Ilya O Tolstikhin, Neil Houlsby, Alexander Kolesnikov, Lucas Beyer, Xiaohua Zhai, Thomas Unterthiner, Jessica Yung, Andreas Steiner, Daniel Keysers, Jakob Uszkoreit, et al. Mlp-mixer: An all-mlp architecture for vision. In *Proceedings of the NeurIPS*, pages 24261–24272, 2021. [5](#), [2](#)
- [38] Önder Tuzcuoğlu, Aybora Köksal, Buğra Sofu, Sinan Kalkan, and A Aydin Alatan. Xoftr: Cross-modal feature matching transformer. In *Proceedings of the CVPR*, pages 4275–4286, 2024. [3](#), [5](#)
- [39] M. Tyszkiewicz, P. Fua, and E. Trulls. Disk: Learning local features with policy gradient. In *Proceedings of the NeurIPS*, pages 14254–14265, 2020. [6](#)
- [40] A. Vaswani, N. Shazeer, N. Parmar, J. Uszkoreit, L. Jones, A. N Gomez, L. Kaiser, and I. Polosukhin. Attention is All you Need. In *Proceedings of the NeurIPS*, pages 5998–6008, 2017. [1](#), [2](#)
- [41] Q. Wang, J. Zhang, K. Yang, K. Peng, and R. Stiefelhagen. Matchformer: Interleaving attention in transformers for feature matching. In *Proceedings of the ACCV*, pages 2746–2762, 2022. [3](#), [6](#), [1](#)
- [42] Yifan Wang, Xingyi He, Sida Peng, Dongli Tan, and Xiaowei Zhou. Efficient loftr: Semi-dense local feature matching with sparse-like speed. In *Proceedings of the CVPR*, pages 21666–21675, 2024. [6](#), [8](#), [1](#)
- [43] Robert L Williams, Douglas A Lawrence, et al. *Linear state-space control systems*. John Wiley & Sons, 2007. [3](#)
- [44] Sanghyun Woo, Shoubhik Debnath, Ronghang Hu, Xinlei Chen, Zhuang Liu, In So Kweon, and Saining Xie. Convnext v2: Co-designing and scaling convnets with masked autoencoders. In *Proceedings of the CVPR*, pages 16133–16142, 2023. [4](#)
- [45] Zichao Zhang, Torsten Sattler, and Davide Scaramuzza. Reference pose generation for long-term visual localization via learned features and view synthesis. *International Journal of Computer Vision*, pages 821–844, 2021. [3](#)
- [46] Lianghui Zhu, Bencheng Liao, Qian Zhang, Xinlong Wang, Wenyu Liu, and Xinggang Wang. Vision mamba: Efficient visual representation learning with bidirectional state space model. *arXiv preprint arXiv:2401.09417*, 2024. [2](#), [3](#)

JamMa: Ultra-lightweight Local Feature Matching with Joint Mamba

Supplementary Material

The supplementary material for JamMa is organized as follows: Sec. **A** reports the evaluation setups of pose estimation experiments in the MegaDepth dataset. Sec. **B** provides additional details on the Mamba block and MLP-Mixer employed in JamMa. Sec. **C** presents further qualitative and quantitative experiments, along with discussions.

Category	Method	Image	Keypoint	Match
Sparse	XFeat	1600	4096	-
	SP + SG	1600	2048	-
	SP + LG	1600	2048	-
	DeDoDe _B	784	10000	-
	DeDoDe _G	784	10000	-
Dense	All	672	-	5000
Semi-Dense	All	832	-	-

Table S1. Evaluation Setups in the MegaDepth [19] Dataset.

A. MegaDepth Setups

As shown in Tab. **S1**, we follow the evaluation setup specified for each method to optimize their performance. For XFeat, images are resized such that the larger dimension is 1600 pixels, with 4096 keypoints extracted per image. For SuperGlue and LightGlue, the larger dimension is similarly resized to 1600 pixels, and 2048 SuperPoint keypoints are extracted per image. For DeDoDe, images are resized to 784×784 , with 10000 keypoints extracted per image. For the dense methods DKM and RoMa, images are resized to 674×674 , and 5000 balanced matches are sampled using the KDE-based method introduced by DKM. For all semi-dense methods [5, 36, 41, 42], images are resized and padded to 832×832 . In the efficiency evaluation, we report the parameters, FLOPs and runtime of the full sparse matching pipelines, including detection, description and matching. All methods utilize LO-RANSAC with an inlier threshold of 0.5 for pose estimation.

B. Details

B.1. Mamba Block

Details of the Mamba block [14] are provided in Fig. **S1** and Alg. **S1**. B and N denote the batch size and sequence length, respectively. C_1 denotes the coarse feature dimension, which is 256. The SSM dimension C_s is set to 16, and the expanded state dimension C_e is set to 512. The input sequence S is first normalized by the layer normalization LN and then linearly projected to X' and Z , both with a dimension size of C_e . A 1D convolution followed by the SiLU nonlinearity is applied

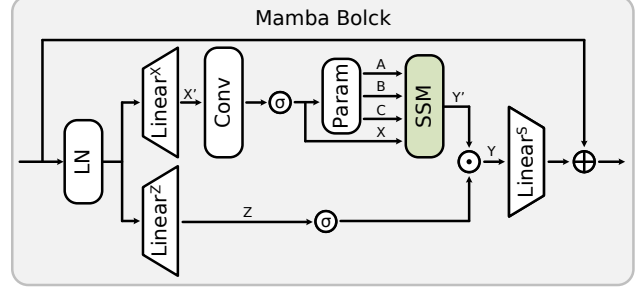


Figure S1. Mamba Block.

Algorithm S1 Mamba Block

Require: input sequence $S : (B, N, C_1)$
Ensure: output sequence $\tilde{S} : (B, N, C_1)$

- 1: $S' : (B, N, C_1) \leftarrow \text{LayerNorm}(S)$
- 2: $X' : (B, N, C_e) \leftarrow \text{Linear}^X(S')$
- 3: $Z : (B, N, C_e) \leftarrow \text{Linear}^Z(S')$
- 4: $X : (B, N, C_e) \leftarrow \text{SiLU}(\text{Conv}(X'))$
- 5: /* compute SSM parameters, "Param" in Fig. S1 */
- 6: $P^\Delta : (B, N, C_e) \leftarrow \text{Parameter}$
- 7: $\Delta : (B, N, C_e) \leftarrow \text{Softplus}(\text{Linear}^\Delta(X) + P^\Delta)$
- 8: $A' : (C_e, C_s) \leftarrow \text{Parameter}$
- 9: $B' : (B, N, C_s) \leftarrow \text{Linear}^B(X)$
- 10: $A, B : (B, N, C_e, C_s) \leftarrow \text{Discretize}(A', B', \Delta)$
- 11: $C : (B, N, C_s) \leftarrow \text{Linear}^C(X)$
- 12: /* SSM recurrent*/
- 13: $h : (B, C_e, C_s) \leftarrow \text{zeros}(B, C_e, C_s)$
- 14: $Y : (B, N, C_e) \leftarrow \text{zeros}(B, N, C_e)$
- 15: **for** i in $\{0, \dots, N-1\}$ **do**
- 16: $h = A[:, i, :, :]h + B[:, i, :, :]X[:, i, :, \text{None}]$
- 17: $Y'[:, i, :] = hC[:, i, :]$
- 18: **end for**
- 19: /* get gated Y */
- 20: $Y : (B, N, C_e) \leftarrow Y' \odot \text{SiLU}(Z)$
- 21: /* residual connection */
- 22: $\tilde{S} : (B, N, C_1) \leftarrow \text{Linear}^S(Y) + S$
- 23: **Return:** \tilde{S}

to X' , producing X , which is then linearly projected to B' , C , and Δ . Δ is used to discretize A' and B' , resulting in A and B . The state-space model (SSM) computes Y' , which is then gated by Z to generate Y . The output sequence \tilde{S} is obtained through the residual connection of Y and S .

Note that the for loop in Alg. **S1**, *i.e.*, SSM recurrent, can be computed once by a global convolution as

$$K = (CB, CAB, \dots, CA^{N-1}B), \quad (S1)$$

$$Y' = X \otimes K,$$

where \otimes denotes the convolution operation.

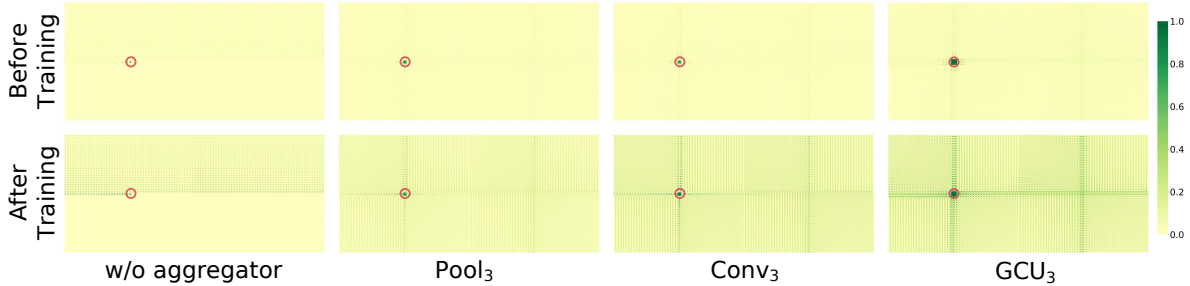


Figure S2. **Effective Receptive Field with Different Aggregators.** All three aggregators expand the local receptive field to a receptive field spread over the image pair.

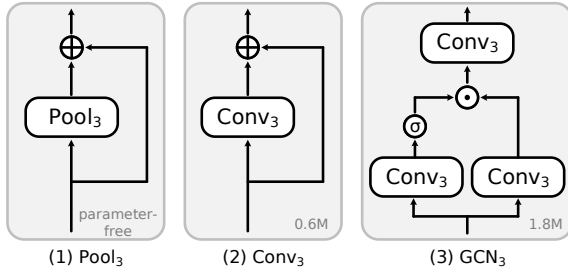


Figure S3. **Three Types of Aggregators.**

B.2. MLP-Mixer

The MLP-Mixer [37] is a purely MLP-based network that first performs spatial mixing using token-wise MLP_s , followed by channel mixing using channel-wise MLP_c .

$$\begin{aligned} F_{mid} &= F_{in} + MLP_s(F_{in}), \\ F_{out} &= F_{mid} + MLP_c(F_{mid}). \end{aligned} \quad (S2)$$

In fine matching module, two 5×5 fine feature windows $\hat{F}_A^f, \hat{F}_B^f \in \mathbb{R}^{M \times 25 \times C_2}$ are spatially concatenated to form $\hat{F}^f \in \mathbb{R}^{M \times 50 \times C_2}$, which is processed by a MLP-Mixer.

In sub-pixel refinement module, two fine features $F_A^s, F_B^s \in \mathbb{R}^{M \times 1 \times C_2}$ are concatenated along the channel dimension, resulting in $F^s \in \mathbb{R}^{M \times 1 \times 2C_2}$. The MLP and Tanh activation are then employed to regress the offsets $\delta_A^x, \delta_A^y, \delta_B^x, \delta_B^y$ of the matching points in images I_A and I_B .

C. More Experiments

C.1. Ablation Study on Aggregator

As shown in Tab. S2 and Fig. S2, we conduct additional ablation studies on the aggregator. We evaluate an average pooling layer with a kernel size of 3, referred to as $Pool_3$, which represents the simplest parameter-free aggregator. As illustrated in Fig. S2, compared to JamMa without an aggregator, $Pool_3$ extends the effective receptive field to a receptive field spread over the image pair. As shown in Tab. S2(1), the minimalist aggregator $Pool_3$ achieves a performance improvement of (+1.0%, +0.8%, +0.9%), validating the importance

Method	Pose est. AUC		
	@5°	@10°	@20°
w/o Aggregator	62.3	75.1	84.3
(1) $Pool_3$	63.3	75.9	85.2
(2) $Conv_3$	64.2	76.9	86.0
(3) GCU_3 (JamMa)	64.5	77.3	86.3

Table S2. **Ablation Study on Aggregator.**

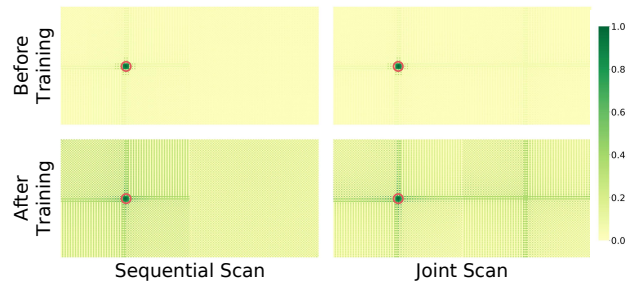


Figure S4. **Effective Receptive Field of Sequential Scan.**

of global dependencies and omnidirectionality. Further performance gains are observed when learnable parameters are incorporated into the aggregators, as shown in Tab. S2(2)(3). Specifically, the gated convolutional unit (GCN_3) improves the performance by (+2.2%, +2.2%, +2%). Additionally, we visualize the effective receptive fields of the models *before training* in Fig. S2. Training allows Mamba to establish long-distance dependencies within sequences, while the aggregator extends the sequence dependencies to global dependencies.

C.2. Effective Receptive Field of Sequential Scan.

As shown in Fig. S4, we compare the effective receptive fields of JamMa using sequential and joint scan. Sequential scan primarily emphasizes internal interactions within a single image but exhibits limited perception of the other image. In contrast, joint scan enables more comprehensive mutual interactions, making it better suited for image matching tasks that require establishing correspondences between *two images*.

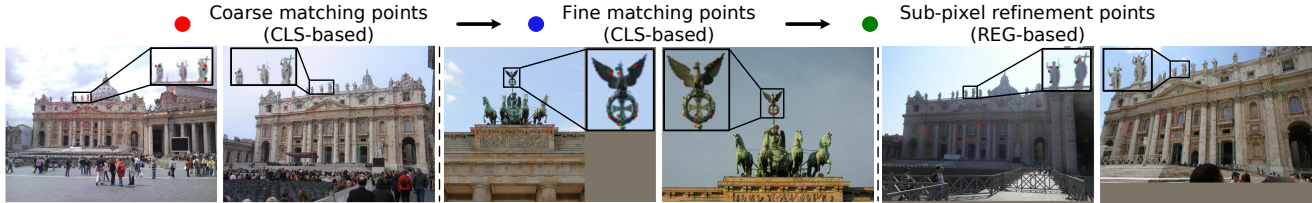


Figure S5. Visualization of the Coarse-to-Fine Matching Module. Zoom in for a clearer view.

Method	Day	Night
	$(0.25m, 2^\circ) / (0.5m, 5^\circ) / (1m, 10^\circ)$	
DeDoDe _B [10]	87.4 / 94.7 / 98.5	70.7 / 88.0 / 97.9
SP [8]+LG [20]	89.6 / 95.8 / 99.2	72.8 / 88.0 / 99.0
LoFTR [36]	88.7 / 95.6 / 99.0	78.5 / 90.6 / 99.0
ASpanFormer [5]	89.4 / 95.6 / 99.0	77.5 / 91.6 / 99.0
JamMa	87.7 / 95.1 / 98.4	73.3 / 91.6 / 99.0

Table S3. Visual Localization on the Aachen Day-Night Benchmark v1.1 [45].

C.3. Visual Localization

Dataset. We evaluate our method on the Aachen Day-Night v1.1 benchmark [45], which includes 824 day-time and 191 night-time images selected as query images for outdoor visual localization.

Metric. We employ the open-source HLoc pipeline [32] for localization and report the percentage of successfully localized images under three error thresholds: $(0.25m, 2^\circ)$, $(0.5m, 5^\circ)$, and $(1m, 10^\circ)$.

Results. As shown in Tab. S3, JamMa demonstrates performance comparable to LoFTR and ASpanFormer in outdoor visual localization tasks. Note that JamMa is significantly more lightweight, achieving over a $2\times$ reduction in parameters and runtime speedup.

C.4. Advantage in Low-Resolution Images.

Quantitative comparisons on low-resolution images are presented in Fig. S6. The results demonstrate that JamMa outperforms ELoFTR by a substantial margin of +15.8% at a resolution of 256, while also achieving higher speed. This highlights JamMa’s potential for resource-constrained applications that demand extreme efficiency (>100 FPS). The superior performance of JamMa in low-resolution scenarios is attributed to shorter input sequences, which alleviate the perceptual attenuation issue of Mamba, *i.e.*, the tendency to overlook distant features within a sequence.

C.5. Visualization of Coarse-to-Fine Module.

We adopt the coarse-to-fine matching module proposed in XoFTR [38], which first performs classification-based (CLS-based) coarse matching on coarse grids, followed by classification-based fine matching on fine grids, and finally regression-based (REG-based) sub-pixel refinement. As shown in Fig. S5, coarse matching on $1/8$ resolution grids of

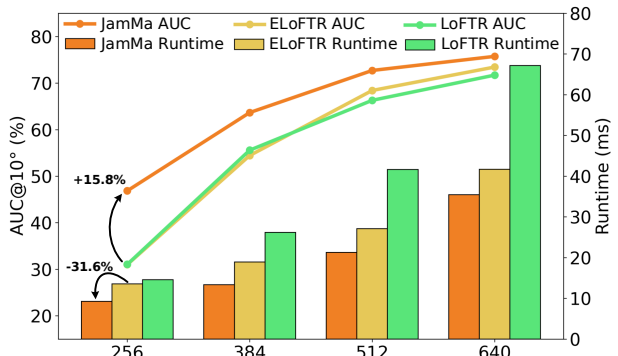


Figure S6. Comparison in Low-Resolution Images.

Method	Time (ms)	Pose est. AUC		
		@5°	@10°	@20°
JamMa	61.8	64.5	77.3	86.3
(1) w/o sub-pixel ref.	60.2	62.1	75.5	84.7
(2) w/ C2F of LoFTR	54.4	61.8	74.9	84.4

Table S4. Ablation Study on Coarse-to-Fine Module. The ref. and C2F denote refinement and coarse-to-fine module, respectively.

ten lacks precision, particularly for small-scale images. Fine matching on $1/2$ resolution grids significantly enhances precision, while regression-based refinement further improves accuracy to the sub-pixel level.

C.6. Ablation Study on Coarse-to-Fine Module

We evaluate the coarse-to-fine module in LoFTR and the coarse-to-fine module in XoFTR without sub-pixel refinement. As shown in Tab. 4(1), sub-pixel refinement supervised by epipolar distance enhances performance by allowing regression-based matching points to achieve sub-pixel accuracy. Although the coarse-to-fine module in LoFTR is faster, its performance is hindered by two key limitations: 1) one-to-one coarse matching struggles in scenes with significant scale variations, and 2) its fine matching does not adjust matching points in the source image.

C.7. More Qualitative Comparisons

We provide additional qualitative comparisons of JamMa with LightGlue and ELoFTR in Fig. S9. JamMa consistently delivers robust matching results with shorter runtime, achieving lower pose estimation errors. Further qualitative comparisons for indoor and outdoor scenes are shown in

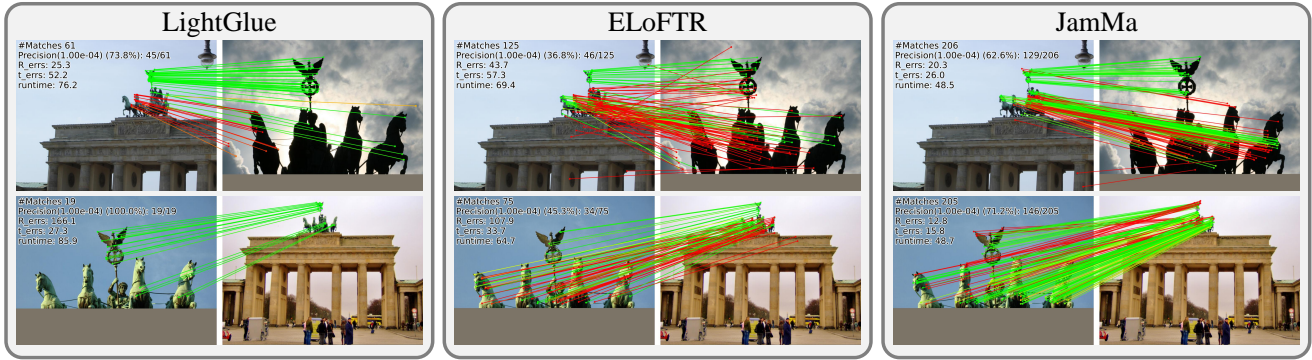


Figure S7. Challenging Scenes.



Figure S8. Failure Cases.

Fig. S10 and Fig. S11, with matched points color-coded for clarity.

C.8. Challenging Scenes.

Qualitative comparisons in challenging scenarios are presented in Fig. S7. All methods exhibit a significant reduction in the number of matches under drastic illumination and scale variations. Nevertheless, JamMa maintains a higher number of correct matches, resulting in more robust pose estimation.

C.9. Failure Cases.

Failure cases of JamMa are illustrated in Fig. S8. These cases typically arise in scenarios with extreme scale and viewpoint variations or in texture-less regions.

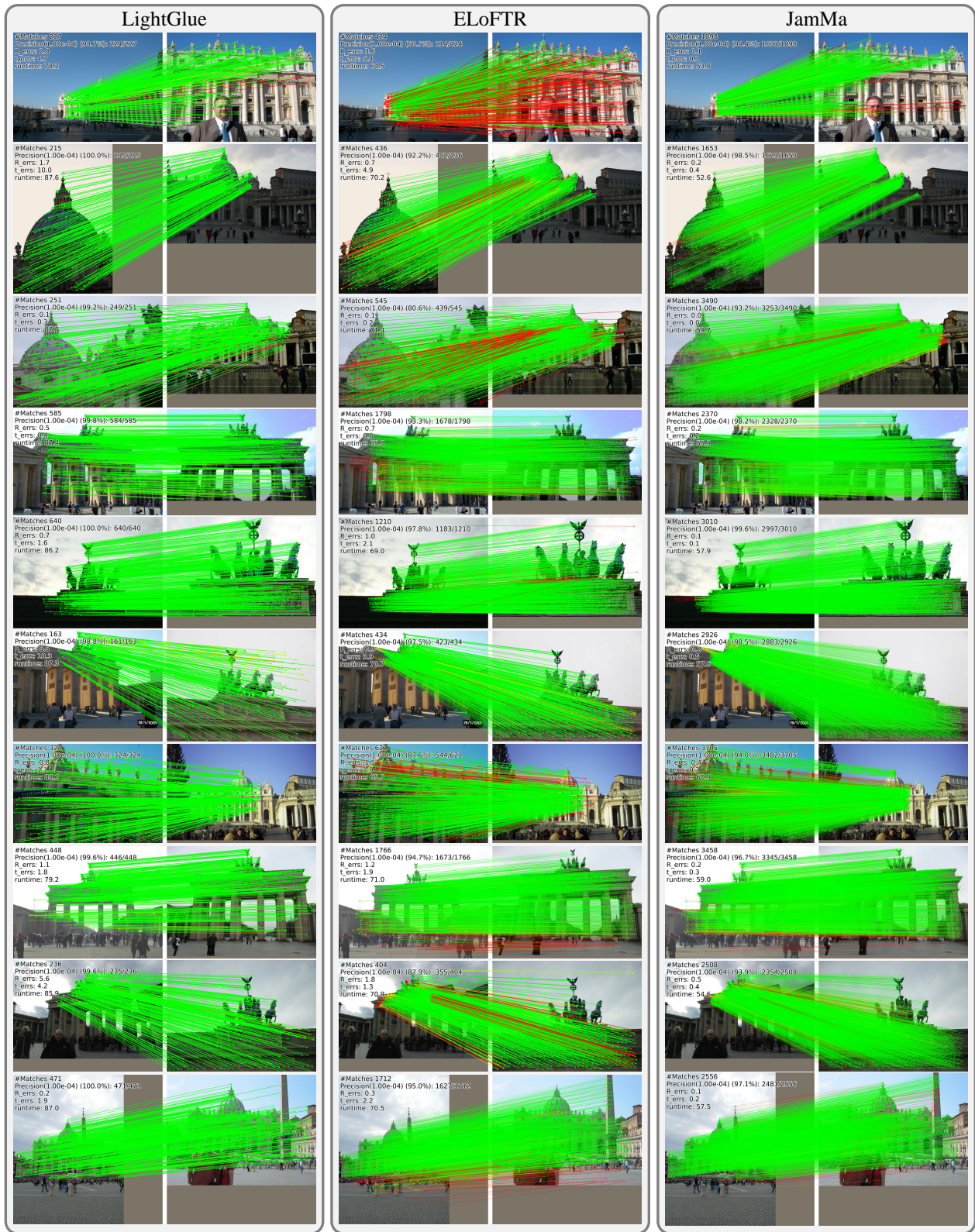


Figure S9. **Comparison of qualitative results.** The reported metrics include precision with an epipolar error threshold of 1×10^{-4} , rotation and translation errors in pose estimation, and runtime.

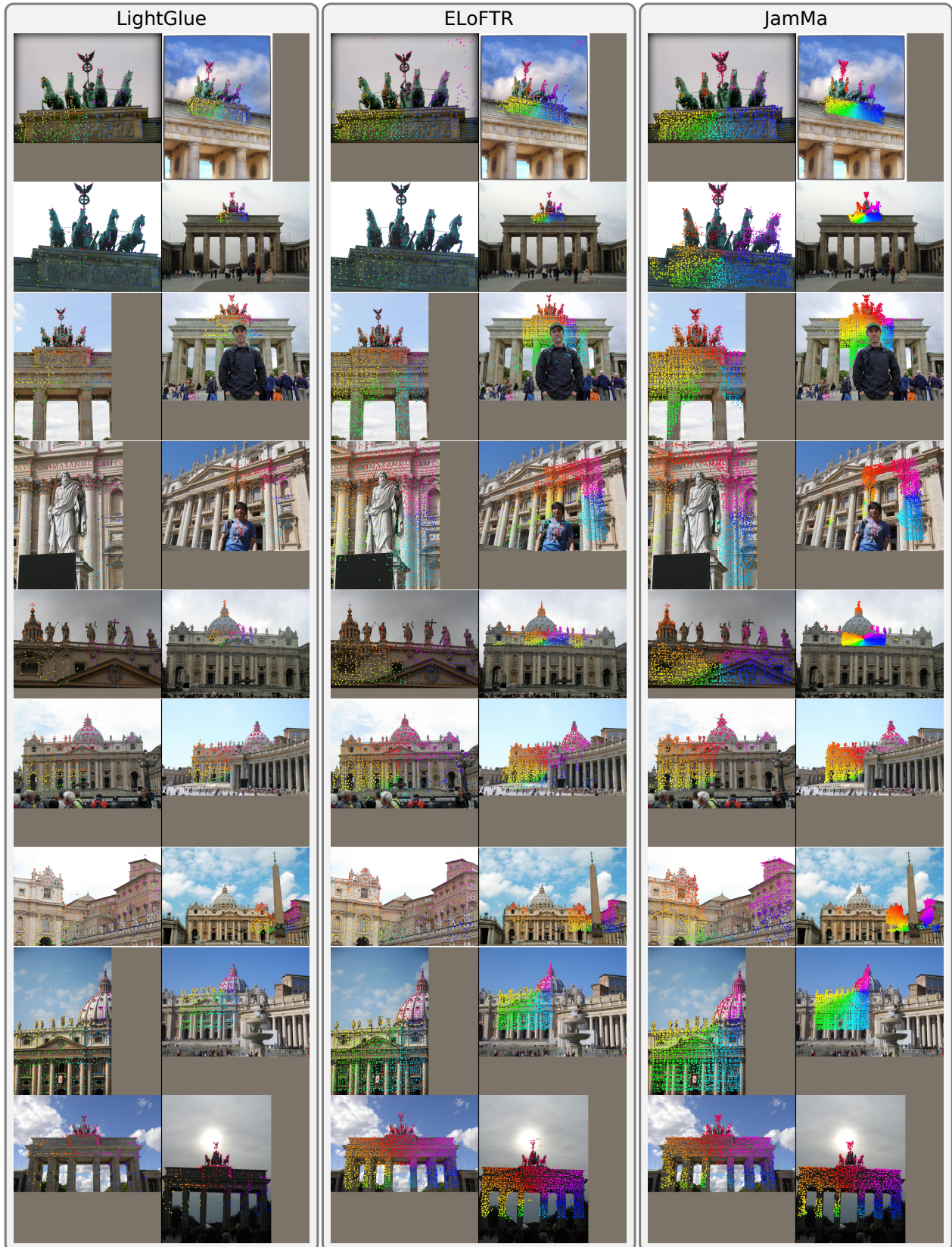


Figure S10. Additional qualitative comparisons in outdoor scenes. The matched points are visualized as the same color.

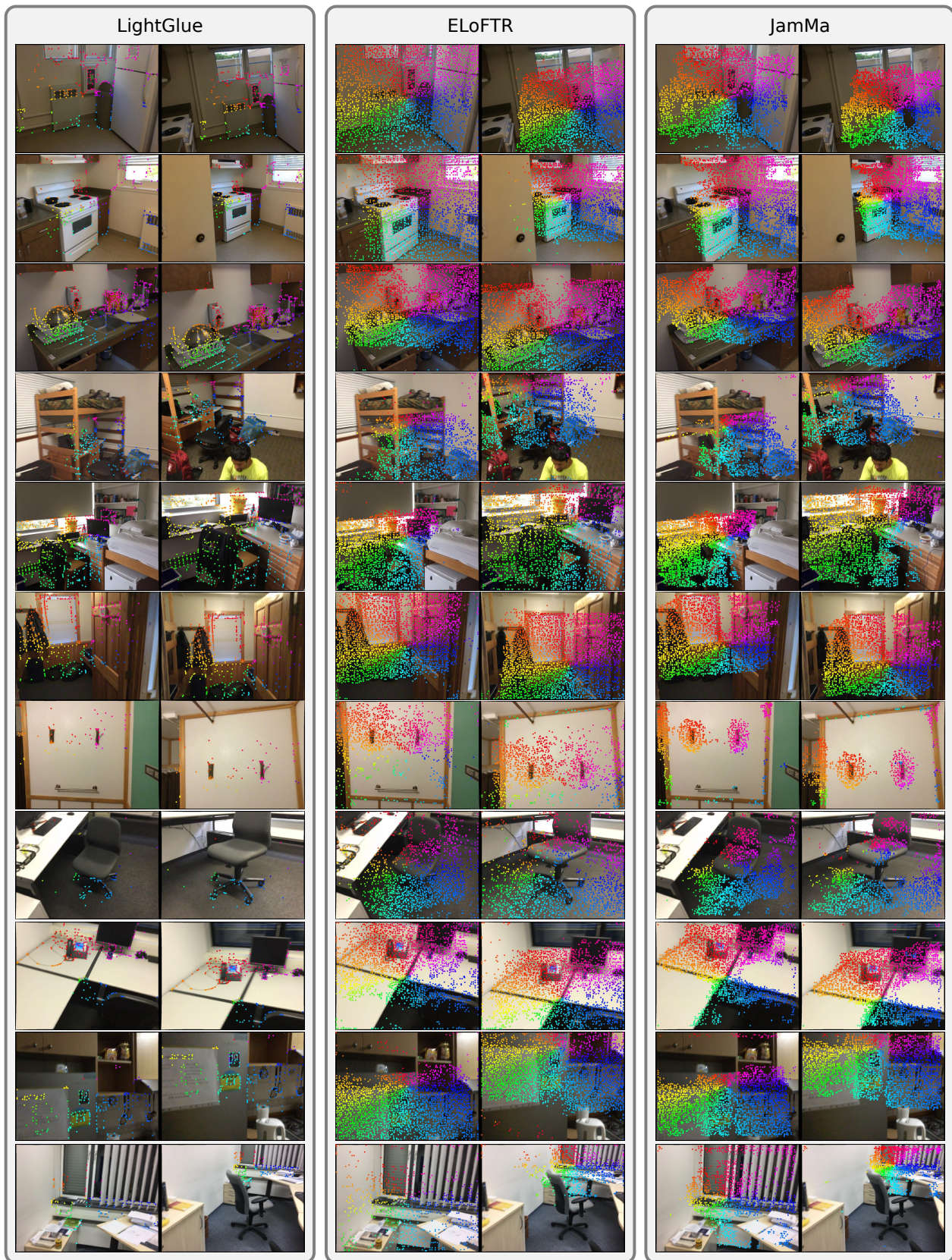


Figure S11. Additional qualitative comparisons in indoor scenes. The matched points are visualized as the same color.